Donor-Acceptor Metallopolymers Containing Ferrocene for Brain Inspired Memristive Devices

Miaocheng Zhang, Chenxi Ma, Dawei Du, Jing Xiang, Suhao Yao, Ertao Hu, Shujuan Liu, Yi Tong, Wai-Yeung Wong,* and Qiang Zhao**

C. Ma, S. Liu, Q. Zhao*
Key Laboratory for Organic Electronics and Information Displays & Jiangsu Key Laboratory for Biosensors, Institute of Advanced Materials (IAM), Nanjing University of Posts and Telecommunications (NJUPT)
9 Wenyuan Road, Nanjing 210023, Jiangsu, P.R. China
E-mail: iamqzhao@njupt.edu.cn
M. Zhang, D. Du, S. Yao, E. Hu, Y. Tong*, Q. Zhao*
College of Electronic and Optical Engineering & College of Microelectronics, Institute of Flexible Electroncs (Future Technology), Nanjing University of Posts and Telecommunications (NJUPT)
9 Wenyuan Road, Nanjing 210023, Jiangsu, P.R. China
E-mail: tongyi@njupt.edu.cn
W.-Y. Wong*
Department of Applied Biology and Chemical Technology, The Hong Kong Polytechnic University (PolyU)
Hung Hom, Hong Kong, P. R. China
PolyU Shenzhen Research Institute
Shenzhen 518057, P. R. China
E-mail: wai-yeung.wong@polyu.edu.hk
J. Xiang, W.-Y. Wong*
Department of Chemistry, Hong Kong Baptist University
Waterloo Road, Hong Kong, P. R. China

Keywords: donor-acceptor, metallopolymer, memristor, brain-inspired systems, memory device

Abstract

To realize brain-inspired devices and systems, memristor is one of the significant alternatives in breaking through the infrastructure restrictions of present logic and memory devices. Organic materials have become popular to fabricate memristive devices due to their unique properties of low cost, mechanical flexibility, and compatibility with complementary metal-oxide-semiconductor technology. Metallopolymer is a new kind of promising organic materials functioning as the resistive-switching layers of memristive devices due to the unique donor-acceptor type structure, which performs good ability of tuning electron concentration to boost the migration of inner ions. Herein, a new metallopolymer MP1 containing ferrocene

and triphenylamine has been designed and synthesized, which was utilized as a resistive-switching layer of memristor with active and inert electrodes of Ag and Pt, respectively. Process flow of devices has been fully developed and MP1 has been found to act as metal-ions-accommodation site with the great potential to boost the formation of conductive filaments in the active region. More interestingly, the conductance of Ag/MP1/Pt memristor can be modulated under various voltage pulses exhibiting distinguished electrical properties. Additionally, synaptic functions have been successfully emulated using such MP1-based memristors. This work will greatly expand the further development of organic memristors for flexible brain-inspired systems.

1. Introduction

Recently, the traditional Von Neumann computing system has severely limited the further development of artificial intelligence (AI) due to its low efficiency in transferring and processing massive data. Memristive devices (*i.e.* memristors) have a huge potential for developing novel highly-efficient brain-inspired computing system,[1-7] which is considered as a promising candidate to replace the present computing system. Memristor exhibits excellent properties, *e.g.* simple structure,[8] multiple resistance states,[9] fast switching speed,[10] and good scalability,[11] which are very beneficial as the building block of future brain-inspired systems. Physical mechanism of memristor has been widely studied and the resistance change is mainly attributed to the formation and dissolution of filaments in the resistance-switching layer between two metal electrodes.[12]

Recently, organic polymer materials as the resistance-switching layers of memristive devices have been reported,[13-16] with excellent memory properties of large switching ratio,[17] low operating voltage,[18] low cost,[19] and mechanical flexibility.[20] However, the organic memristive devices usually encounter rigorous issues of low stability due to the uncertain redox properties within organic polymer materials.[14,19] On the other hand, polymers with the typical donor-acceptor (D-A) type can adjust their micro-structure to boost inner ion migration,[21-24] which plays an important role in the formation of conductive filaments of memristive devices. It has been reported that metal-containing polymers[57-66] actually belong to a new kind of D-A polymers.[25-30] Nevertheless, the explorations of using novel D-A type metal-containing polymers in memristors are extremely rare.[31-32] It will be very useful to investigate the effects of D-A type metal-containing polymers on the performance of memristors utilizing the excellent redox properties of metal center. The study of biological response for memristor of D-A type metal-containing polymers needs to be further explored as well.[53-56]

In this work, we designed and synthesized a novel D-A type metal-containing conjugated polymer MP1 by copolymerizing the ferrocene and triphenylamine monomers.[3,33] In addition, the structure was determined by nuclear magnetic resonance. The polymer has been introduced to memristor as the resistive-switching layer, and the whole process flow has been developed. The Ag/MP1/Pt memristors with crossbar structures have been successfully fabricated using the traditional silicon-based semiconductor fabrication process. The resistive-switching characteristics have been clearly observed. The D-A type metal-containing conjugated polymer MP1 can benefit the formation of conductive filaments and act as metal-ions-accommodation site of memristors.[34,52]. Moreover, the memristors are able to possess good stability, and the retention of the resistance of on state (R_{on}) and off state (R_{off}) has been studied in details. Apart from the direct-current (D. C.) test, continuous pulse voltage signal has been applied to MP1 devices as well. Additionally, the emulation of the biological response of the human brain can be successfully realized, particularly the enhancement of short-time memory ability and paired-pulse facilitation (PPF) behavior. The results reported in this work will further contribute to the application of organic polymers in brain-inspired devices and systems in the future.

2. Results and discussion

2.1. Design and Synthesis of MP1

Continuous resistance switching characteristics are the key to achieve multi-level storage for memristors. The designed D-A polymer contains multiple redox active units, and its continuous redox behavior will cumulatively change the electronic structure and conductivity of the material.[25,51] So, the D-A polymer MP1 has been introduced to the resistive-switching layer of memristor in the work. Ferrocene is a typical material with redox properties, and triphenylamine is rich in electrons. So as shown in **Scheme 1**, ferrocene and triphenylamine are used as raw materials. MP1 is based on the triphenylamine modified skeleton which contains a ferrocene center in the repeating unit. The ferrocene center in this structure can not

only provide an effective redox conductivity site, but also provide a thermodynamic sink to capture/locate charges due to the introduction of a low energy state.[25] This structural design of electronic interaction will provide more probabilities in the application of memristive devices.

The synthetic routes of 1,1'-diiodoferrocene (FcI_2), 4-ethynyl-N-(4-ethynylphenyl)-N-phenylaniline (DEnTPA), and MP1 are shown in **Scheme 1**. FcI_2 was prepared by the reported one-pot method.[27-29] For DEnTPA, N-phenyl-4-((trimethylsilyl)ethynyl)-N-(4-(trimethylsilyl)-ethynyl)phenyl)aniline DEnTPA-1 was firstly synthesized according to the literature method,[30] followed by processing DEnTPA-1 to obtain DEnTPA. Finally, in the presence of tetrakis(triphenylphosphine)palladium(0) and copper(I) iodide, a ferrocene-embedded metallopolymer MP1 was synthesized through the Sonogashira cross-coupling polycondensation reaction of FcI_2 and DEnTPA.[25-29] The new intermediates and MP1 were characterized by nuclear magnetic resonance (^{1}H NMR and $^{13}C\{^1H\}$ NMR).

2.2. Physical characteristics of MP1

The optical features of MP1 were investigated by UV-Vis absorption (**Figure S4**a) and emission spectroscopy (**Figure S4**b). As is shown in **Figure S4**a, MP1 has two absorption peaks near 290 nm and 350 nm, corresponding to the π-π* electronic transition from the terminal ferrocene and triphenylamine moiety, respectively. As is shown in **Figure S4**b, the maximum emission peak of MP1 is about 450 nm. Moreover, the cyclic voltammetry (CV) curve of MP1 was explored (**Figure S5**). As is shown in **Figure S5**, this stack up phenomenon is also appeared in the CV curve of the ferrocene-containing polytriphenylamine PTPAFc reported by Zhang *et al.*[67] However, the reversible redox peaks of ferrocene and triphenyl amine entities were not shown as expected in MP1, which may be caused by the irreversible characteristic coupling reaction of the triphenylamine unit. When the CV scanning is extended to 1.5 V, the triphenylamine moiety could be oxidized, which may lead to a positive charge at the free para-position of one phenyl ring attached to the triarylamine

and enable oxidative coupling. This irreversible characteristic coupling reaction of the triphenylamine unit could further result in the structural change of partial triphenylamine moiety.[68] After the oxidation activation, a more stabilized cross-linked structure was formed which leads to a stable current in the following CV scanning process.

2.3 Physical characterization of Ag/MP1/Pt memristor

The fabrication process of the memristive devices with crossbar structure is schematically shown in **Figure 1**a. The prepared Ag/MP1/Pt memristor was characterized by SEM to observe the internal crossbar structure. The SEM picture is shown in **Figure 1**b. The vertical crossbar structures can be observed obviously. The grey line is the Ag top electrode and the light-white line is the Pt bottom electrode. Each vertically overlapping part is one memristor. The prepared Ag/MP1/Pt memristor was also characterized by the optical microscope, as shown in **Figure 1**c. The scale bar is 500 μm. The Ag top electrode and the Pt bottom electrode can be clearly observed. In order to figure out the thickness of the organic MP1 film, a test by the typical profilometer of DektakXT Bruker was conducted as shown in **Figure S1**. It can be observed that the average thickness of MP1 film is about 27.96 nm. This indicates that the process of preparation can be suitably applied to the industrial production. In order to figure out the uniformity of the MP1 film in the experiment, a three-dimensional atomic force microscope (AFM) image of MP1 is shown in **Figure 1**d. It can be observed that the MP1 film has been prepared uniformly on the substrate.

2.4 Electrical characteristics of MP1 memristor

The electrical characteristics of MP1 memristors were measured by the Keithley 4200A semiconductor analyzer. During the measurement process, the silver (Ag) top electrode was applied with positive bias, while the Pt bottom electrode was grounded. **Figure 2**a shows the current-voltage (*I-V)* curve of the initial forming process of Ag/MP1/Pt memristor. The electroforming process usually needs a large voltage to promote the formation of conductive filaments. It can be observed in **Figure 2**a that when the initially applied voltage increases

from 0 V to 3 V, the Ag/MP1/Pt device is tuned from the high resistance state (HRS) to the low resistance state (LRS) and the working current increases obviously. Then, when the applied voltage decreases from 3 V to 0 V, the working current is proportionally reduced, which indicates that this memristor is maintained at the LRS due to the forming of conductive filaments.[35]

After the forming process, a double-sweep-voltage was applied to the device to measure its *I-V* characteristics. As a result, resistive-switching behavior can be clearly observed under dual voltage sweeps. The *I-V* curve in **Figure 2**b shows that when the applied voltage increases from 0 V to 2 V, the resistance of the device is shifted from the HRS to the LRS and the working current increases obviously, *i.e.* the SET process.[36] By applying a negative voltage sweeping from 0 V to -3 V, the resistive state of the device returns to the HRS from the LRS, *i.e.* the RESET process.[37] The switching ratio of R_{on}/R_{off} for the device is ~10^3, which can be potentially used for the industry.

The further applications of memristor need the devices possessing the ability of long-term memory (LTM). So, the data retention of Ag/MP1/Pt has been measured and shown in **Figure 2**c. The black symbol and line represent R_{on}, while the red symbol and line represent R_{off}. The time of R_{on} and R_{off} can last for about 5000 s. The R_{on}/R_{off} ratio of Ag/MP1/Pt memristor is higher than that of the Ag/MP1/SiO_2/Pt memristor shown in **Figure S8**. The detailed data of electrical characteristics of the Ag/MP1/SiO_2/Pt memristor have been shown in the Supporting Information.[38]

The classical nonlinear conductive mechanisms of memristive device include the Poole-Frenkel (PF) emission, Schottky-like emission, and space charge limited current (SCLC).[38] To determine the conductive mechanism of the Ag/MP1/Pt memristor, the double-logarithmic *I-V* curves and the linear fits to the SET and RESET process are plotted in **Figure 2**e,f. At the low voltage region, the current is dependent on the voltage, obeying the ohmic conduction with the linear relationship. At the high voltage region, a sharp increase of current with the

increased voltage indicates that the Ag/MP1/Pt device switches to the LRS. The *I-V* behavior follows Child's law ($I \sim V^2$). Therefore, the resistive switching mechanism is in agreement with the SCLC model,[39-40] revealing the filaments model.

According to the analysis of conduction mechanism of memristor, as shown in **Figure 2**d, when the Ag top electrode is applied with a positive voltage, the Ag atom will be oxidized: $Ag \rightarrow Ag^+ + e^-$. It has been found that MP1 may act as metal-ions-accommodation site and help the formation of conductive filaments in the active region. Due to the presence of an applied voltage, there is an electric field inside the device from the top electrode to the bottom electrode. Electrons move toward the positive voltage source, and Ag^+ ions move toward the bottom electrode along the electric field.[49] When Ag^+ ions reach the bottom electrode (Pt), the following chemical reaction near the bottom electrode will occur: $Ag^+ + e^- \rightarrow Ag$.[39-40] As the reaction proceeds, the Ag atoms gradually reach a nucleation near the bottom electrode and extend toward the top electrode. When the stacked Ag atoms completely connect the top and bottom electrodes, the device will change from the HRS to the LRS. The conductive channels formed by the Ag atoms are called conductive filaments.[47-48]

2.5 The emulation of the biological synaptic responses of the human brain using MP1 memristor

2.5.1 The enhancement of transition from short-term memory to long-term memory

To observe the memory ability,[41-42] forty large voltage pulses with the amplitude of 1 V, 2 V and 3 V were used to stimulate the device, respectively. Immediately, small voltage pulses of 0.1 V were applied to measure the conductivity change of the device. The results are shown in **Figure** 3. When the amplitude of applied voltage pulse is 1 V, the memristor has not been stimulated to open. The conductivity of the device declines only after 65 ms. But when the amplitude of the applied voltage is 3 V, the device conductance can be stimulated larger than that by being applied with 1 V pulses. The duration of the high conductance state can reach ~1000 ms. The enhancement of transition from short-term memory to long-term memory can be observed with the increase of the amplitude of the applied voltage pulse. The phenomena

are consistent with synaptic responses in the human brain where the larger the external stimulus is applied, the stronger the synaptic connectivity is. In addition, forty large voltage pulses with amplitudes of 1 V, 3 V and 5 V were applied to the Ag/MP1/SiO_2/Pt memristor which is shown in **Figure S9**.

2.5.2 Paired-pulse facilitation

From the review of biological systems, short-term plasticity (STP) is important for the neural computation of biological synapses. In biological synapses, calcium ions can enter the endings of the cranial nerves for the rapid production of transmitters, which induces an instantaneous increase of the connections, *i.e.* the STP. Paired-pulse facilitation (PPF) is a typical example of the STP. The conductance of memristor is affected by the internal ion migration, which is similar to the synaptic weights. As shown in **Figure 4**a, when two pulses with the same amplitude of 4 V are applied to the Ag/MP1/Pt memristor,[43-44] the current generated by the second pulse is larger than that generated by the first pulse. The ratio of the amplitudes of the two current spikes is called the PPF index. The PPF index shown in **Figure 4**a is calculated to be 2.5. It can be found that the PPF index increases/decreases with the decrease/increase of the pulse interval, respectively. The red dots in **Figure 4**b plot the relationship between the PPF index and the pulse interval, which can be well fitted by the function of $y = A_1 \times \exp(-\Delta t/t_1) + y_0$, A_1, t_1, and y_0 are constants, Δt is a time interval variable.[45-46] The fitting parameters are shown in **Table S2**. The fitting curve is similar to the curve of the biological synaptic responses.

3. Conclusions

In summary, a new strategy was proposed to successfully synthesize the novel D-A ferrocene-containing metallopolymer MP1 for brain inspired memristive devices. In addition, the Ag/MP1/Pt and Ag/MP1/SiO_2/Pt memristors have been successfully fabricated. The metallopolymer MP1 was used as the resistive-switching layer and the insertion of SiO_2 can reduce power consumption which is the most challenging task for the brain-inspired system.

The hysteresis curves were achieved in both Ag/MP1/Pt and Ag/MP1/SiO_2/Pt devices. Moreover, the continuous pulses were applied to the Ag/MP1/Pt memristor to simulate the synaptic behaviors of human brain, including the transition from short to long-term memories and paired-pulse facilitation. This work will further promote the development of organic and polymeric D-A memristors in the brain-inspired system.

4. Experimental section

4.1. Synthesis of MP1

Synthesis and Characterization of **MP1**:[5] To a mixture of DEnTPA (40 mg, 0.136 mmol) and FcI_2 (60 mg, 0.136 mmol) in a mixed solution of triethylamine (10 mL) and dry THF (10 mL) under nitrogen were added copper iodide (2 mg, 0.0068 mmol) and tetrakis(triphenylphosphine)palladium (8 mg, 0.0068 mmol). After being stirred for 30 min at r. t., the mixture was then heated to reflux overnight. When the reaction was complete, the mixture was cooled down to r. t., and the solvent was then removed under reduced pressure. The residue was chromatographed over a silica gel column by eluting with dichloromethane and methanol to give a red solid, which was precipitated in hexane to afford the desired compound (60%). The number-average molecular weight (M_n) is 5.6×10^3 g mol^{-1}, weight-average molecular weight (M_w) is 9.7×10^3 g mol^{-1}, and polydispersity index (PDI) is 1.7. ^{1}H NMR (tetrahydrofuran-d_8, 400 MHz): δ 7.96~6.99 (m, ArH), 5.05~4.23 (m, FcH). FT-IR (KBr pellet, cm^{-1}): 3054 (C-H stretching, Fc), 2196 (C≡C stretching), 1590 (C=C stretching, Ar), 1500 (C=C stretching, Ar), 1288 (C-N stretching, Ar), 1110 (C-C stretching, Fc), 1035 (C-C stretching, Fc), 832 (C-H bending, Fc), 493 (C-Fc stretching, Fc). The ^{1}H NMR spectrum of MP1 is shown in **Figure S3**. As is shown in the figure, the broadened peak at δ = 8.00-6.50 ppm is attributed to the aromatic phenyl protons, while the characteristic signal at δ = 5.10-4.00 ppm is attributed to the ferrocene moiety.

4.2. Device fabrication

Firstly, the wafers were cleaned using dilute hydrofluoric acid and deionized water. Next, 80-nm-thick platinum (Pt) was deposited onto the Si substrate as the bottom electrode through a shadow mask by physical vapor deposition (PVD) with electron beam assisted sputter. After that, the MP1 resistive-switching layer was deposited by spin-coating, followed by a thermal annealing process. Finally, 80-nm-thick metallic Ag was deposited through a shadow-mask as the top electrode by PVD with electron beam assisted sputtering. The final Ag/MP1/Pt memristors with the two-terminal structure were characterized by using the scanning electron microscope and optical microscope. In addition, the Ag/MP1/SiO_2/Pt has been fabricated for comparison. The 50 nm SiO_2 was deposited between MP1 layer and Pt layer by PVD with electron beam assisted sputtering. The other layers were deposited with the same process as for Ag/MP1/Pt.

Supporting Information

Supporting Information is available from the Wiley Online Library or from the author.

Acknowledgements

Miaocheng Zhang and Chenxi Ma contributed equally to this work. All the authors have given approval to the final version of the manuscript. This work was supported in part by the National Funds for Distinguished Young Scientists (61825503), Postgraduate Research & Practice Innovation Program of Jiangsu Province (KYCX19_0956, KYCX19_0960, SJCX19_0268), National Natural Science Foundation of China (61804079, 61904087), the Science, Technology and Innovation Committee of Shenzhen Municipality (JCYJ20180507183413211), the Hong Kong Research Grants Council (PolyU 153051/17P), the Hong Kong Polytechnic University (1-ZE1C), the Endowed Professorship in Energy from Ms Clarea Au (847S), Jiangsu Province Research Foundation (BK20191202,

NLXZYZZ219001, RK106STP18003, SZDG2018007, CZ1060619001), NJUPTSF (NY218107, NY220078).

Received: ((will be filled in by the editorial staff))
Revised: ((will be filled in by the editorial staff))
Published online: ((will be filled in by the editorial staff))

References:

[1] B. S. Dmitri, S. S. Gregory, R. S. Duncan, R. S. Williams, *Nature* **2008**, *453*, 80.

[2] Y. LeCun, Y. Bengio, G. Hinton, *Nature* **2015,** *521*, 436.

[3] C. H. Wang, W. He, Y. Tong, Y. S. Zhang, K. J. Huang, L. Song, S. Zhong, R. Ganeshkumar, R. Zhao, *Small* **2017**, *13*, 1603435.

[4] M. Prezioso, F. Merrikh-Bayat, B. D. Hoskins, G. C. Adam, K. K. Likharev, D. B. Strukov, *Nature* **2015**, *521*, 61.

[5] D. Li, B. Wu, X. J. zhu, J. T. Wang, B. Ryu, W. D. Lu, W. Lu, X. G. Liang, *ACS Nano* **2018**, *12*, 9240.

[6] Y. Li, S. B. Long, Q. Liu, H. B. Lv, M. Liu, *Small* **2017**, *13*, 1604306.

[7] Y. J. Jeong, J. Lee, J. Moon, J. H. Shin, W. D. Lu, *Nano Lett.* **2018**, *18*, 4447.

[8] D. B. Strukov, R. S. Williams, *Appl. Phys. A* **2009**, *94*,515.

[9] Y. H. Yin, Z. D. Liu, M. Y. Song, S. Ju, X. J. Wang, Z. Zhou, H. W. Mao, Y. M. Ding, J. Q. Liu, W. Huang, *J. Mater. Chem. C* **2018**, *6*, 11162.

[10] J. H. Nickel, J. P. Strachan, M. D. Pickett, C. T. Schamp, J. J. Yang, J. A. Graha, R. S. Williams, *Microelectron. Eng.* **2013**, *103*, 66.

[11] Dmitri B. Strukov, Tightening grip, *Nat. Mater*. **2018**, *17*, 293.

[12] P. Salles, E. Quain, N. Kurra, A. Sarycheva, Y. Gogotsi, *Small* **2018**, *14*, 1802864.

[13] A. S. Sokolov, M. Ali, R. Riaz, Y. Abbas, M. J. Ko, C. Choi, *Adv. Funct. Mater.* **2019,** *29*, 1807504.

[14] Z. Y. Lv, Q. K. Hu, Z.-X. Xu, J. J. Wang, Z. H. Chen, Y. Wang, M. Chen, K. Zhou, Y.

Zhou, S. T. Han, *Adv. Electron. Mater.* **2019**, 1800793.

[15] S. Song, B. Cho, T.-W. Kim, Y. Ji, M. Jo, G. Wang, M. Choe, Y. H. Kahng, H. Hwang, T. Lee, *Adv. Mater.* **2010**, *22*, 5048.

[16] F. C. Zhou, Z. Zhou, J. W. Chen, T. H. Choy, J. L. Wang, N. Zhang, Z. Y. Lin, S. M. Yu, J. F. Kang, H.-S. P. Wong, Y. Chai, *Nat. Nanotechnol.* **2019**, *14*, 776.

[17] S.-H. Lee, H.-L. Park, C.-M. Keum, I.-H. Lee, M.-H. Kim, S.-D. Lee, *Phys. Status Solidi RRL* **2019**, 1900044.

[18] D. A. Lapkin, S. N. Malakhov, V. A. Demin, S. N. Chvalun, L. A. Feigin, *Synth. Met.* **2019**, *254*, 63.

[19] A. A. Minnekhanov, A. V. Emelyanov, D. A. Lapkin, K. E. Nikiruy, B. S. Shvetsov, A. A. Nesmelov, V. V. Rylkov, V. A. Demin, V. V. Erokhin, *Sci. Rep.* **2019**, *9*, 10800.

[20] S. A. Hadi, K. M. Humood, M. A. Jaoude, H. Abunahla, H. F. A. Shehhi, B. Mohammad, *Sci. Rep.* **2019**, *9*, 9983.

[21] C. Wang, G. Liu, Y. Chen, R.-W. Li, W. B. Zhang, L. X. Wang, B. Zhang, *J. Mater. Chem. C* **2015**, *3*, 664.

[22] R. N. Arunagirinathan, P. Gopikrishna, D. Das, P. K. Iyer, *ACS Appl. Electron. Mater.* **2019**, *1*, 600.

[23] W.-Y. Lee, T. Kurosawa, S.-T. Lin, T. Higashihara, M. Ueda, W.-C. Chen, *Chem. Mater.* **2011**, *23*, 4487.

[24] C.-T. Poon, D. Wu, W. H. Lam, V. W.-W Yam, *Angew. Chem. Int. Ed.* **2015**, *54*, 10569.

[25] B. Zhang, F. Fan, W. H. Xue, G. Liu, Y. B. Fu, X. D. Zhuang, X.-H. Xu, J. W. Gu, R.-W. Li, Y. Chen, *Nat. Commun.* **2019**, *10*, 736.

[26] A. K. Palai, S. P. Mishra, A. Kumar, R. Srivastava, M. N. Kamalasanan, M. Patri, *Macromal. Chem. Phys.* **2010**, *211*, 1043.

[27] M. Roemera, C. A. Nijhuis, *Dalton Trans.* **2014**, *42*, 11815.

[28] D. A. Khobragade, S. G. Mahamulkar, L. Pospíšil, I. Císarová, L. Rulíšek, U. Jahn,

Chem. Eur. J. **2012**, *18*, 12267.

[29] M. S. Inkpen, S. Du, M. Driver, T. Albrecht, N. J. Long, *Dalton Trans.* **2013**, *42*, 2813.

[30] Z. Fang, M. Samoc, R. D. Webster, A. Samoc, Y.-H. Lai, *Tetrahedron Lett.* **2012**, *53*, 4885.

[31] I. Boybat, M. L. Gallo, S. R. Nandakumar, T. Moraitis, T. Parnell, T. Tuma, B. Rajendran, Y. Leblebici, A. Sebastian, E. Eleftheriou,, *Nat. Commun.* **2018**, *9*, 2514.

[32] C. Li, D. Belkin, Y. N. Li, P. Yan, M. Hu, N. Ge, H. Jiang, E. Montgomery, P. Lin, Z. R. Wang, W. H. Song, J. P. Strachan, M. Barnell, Q. Wu, R. S. Williams, J. J. Yang, Q. F. Xia, *Nat. Commun*. **2018**, *9*, 2385.

[33] S. Pi, C. Li, H. Jiang, W. W. Xia, H. L. Xin, J. J. Yang, Q. F. Xia, *Nat. Nanotechnol.* **2019**, *14*, 35.

[34] Mi. Kim, S. U. Ryu, S. A. Park, K. Choi, T. Kim, D. Chung, T. Park, *Adv. Funct. Mater.* **2019**, *30*, 1904545.

[35] Y.-H. Ting, J.-Y. Chen, C.-W. Huang, T.-K. Huang, C.-Y. Hsieh, W.-W. Wu, *Small* **2018**, *14*, 1703153.

[36] S. R. Nandakumar, M. Minvielle, S. Nagar, C. Dubourdieu, B. Rajendran, *Nano Lett.* **2016**, *16*, 1602.

[37] W. H. Chen, R. C. Fang, M. B Balaban, W. J. Yu, Y. G.-Velo, H. JBarnaby, M. N. Kozicki, *Nanotechnol.* **2016**, *27*, 255202.

[38] Wang, C.-H. Hsu, Y.-R. Ye, C.-S. Lai, C.-F. Ai, W.-F. Tsai, *IEEE Electron Device Lett.* **2014**, *35*, 4.Y. Zhang, Y. Li, X. P. Wang, E. G. Friedman, *IEEE Electron Device Lett.* **2017**, *64*, 4.

[40] H. Y. Peng, T. Wu, *Appl. Phys. Lett.* **2009**, *95*, 152106.

[41] Y. Li, Y. P. Zhong, L. Xu, J. J. Zhang, X. H. Xu, H. J. Sun, X. S. Miao, *Sci. Rep.* **2013**, *3*, 1619.

[42] R. Yang, H.-M. Huang, Q.-H. Hong, X.-B. Yin, Z.-H. Tan, T. Shi, Y.-X. Zhou, X.-S.

Miao, X.-P. Wang, S.-B. Mi, C.-L. Jia, X. Guo, *Adv. Funct. Mater.* **2017**, 1704455.

[43] Z. Y. Zhang, T. R. Li, Y. J. Wu, Y. J. Jia, C. W. Tan, X. T. Xu, G. R. Wang, J. Lv, W. Zhang, Y. H. He, J. Pei, C. Ma, G. Q. Li, H. Z. Xu, L. P. Shi, H. L. Peng, H. L. Li, *Adv. Mater.* **2019**, *31*, 1805769.

[44] Z. Q. Wang, H. Y. Xu, X. H. Li, H. Yu, Y. C. Liu, X. J. Zhu, *Adv. Funct. Mater.* **2012**, *22*, 2759.

[45] X. B. Yan, L. Zhang, H. W. Chen, X. Y. Li, J. J. Wang, Q. Liu, C. Lu, J. S. Chen, H. Q. Wu, P. Zhou, *Adv. Funct. Mater.* **2018**, 1803728.

[46] X. B. Yan, J. H. Zhao, S. Liu, Z. Y. Zhou, Q. Liu, J. S. Chen, X. Y. Liu, *Adv. Funct. Mater.* **2018**, *28*, 1705320.

[47] X. Guo, C. Schindler,S. Menzel, R. Waser, *Appl. Phys. Lett.* **2007**, *91*, 133513.

[48] S. H. Jo, K. H. Kim., W. Lu, *Nano Lett.* **2009**, *1*, 496.

[49] S. H. Jo, W. Lu, *Nano Lett.* **2008**, *2*, 392.

[50]C.-L. Liu, W.-C. Chen, *Polym. Chem.* **2011**, *2*, 2169.

[51] J. Xiang, X. L. Li, Y. Ma, Q. Zhao, C.-L. Ho, W.-Y. Wong, *J. Mater. Chem. C* **2018**, *6*, 11348.

[52] Lan, G. Zhang, X. Chen, Y. Zhang, K. A. I. Zhang, X. Wang, *Angew. Chem. Int. Ed.* **2019**, *58*, 10236.

[53] Y. Chen, G. Liu, C. Wang, W. Zhang, R. -W. Li, L. Wang, *Mater. Horiz.* **2014**, *1*, 489.

[54] C. Wang, G. Liu, Y. Chen, R. –W. Li, W. Zhang, L. Wang, B, Zhang, *Mater. Chem. C* **2015**, *3*, 664.

[55] X. Yan, J. Wang, M. Zhao, X. Li, H. Wang, L. Zhang, C. Lu, D. Ren, *Appl. Phys. Lett.* **2018**, *113*, 013503.

[56] B, Zhang, C, Wang, L, Wang, Y, Chen, *J. Mater. Chem. C* **2018**, *6*, 4023.

[57] Lovinger, J. Andrew., *Science* **1983**, *220*, 1115.

[58] J. R. Aggas, W. Harrell, J. Lutkenhaus, A. Guiseppi-Elie, *Nanoscale* **2018**, *10*, 672.

[59] Busby, N. Crespo-Monteiro, M. Girleanu, M. Brinkmann, O. Ersen, J. J. Pireaux, *Org. Electron.* **2015**, *16*, 40.

[60] S. Goswami, A. J. Matula, S. P. Rath, S. Hedstrom, S. Saha, M. Annamalai, D. Sengupta, A. Patra, S. Ghosh, H. Jani, S. Sarkar, M. R. Motapothula, C. A. Nijhuis, J. Martin, S. Goswami, V. S. Batista, T. Venkatesan, *Nat. Mater.* **2017**, *16*, 1216.

[61] F. A. A. Nugroho, I. Darmadi, L. Cusinato, A. Susarrey-Arce, H. Schreuders, L. J. Bannenberg, A. B. da Silva Fanta, S. Kadkhodazadeh, J. B. Wagner, T. J. Antosiewicz, A. Hellman, V. P. Zhdanov, B. Dam, C. Langhammer, *Nat. Mater.* **2019**, *18*, 489.

[62] S. Porro, K. Bejtka, A. Jasmin, M. Fontana, G. Milano, A. Chiolerio, C. F. Pirri, C. Ricciardi, *Nanotechnology* **2018**, *29*, 495201.

[63] N. Sanetra, Z. Karipidou, R. Wirtz, N. Knorr, S. Rosselli, G. Nelles, A. Offenhaeusser, D. Mayer, *Adv. Funct. Mater*. **2012**, *22*, 1129.

[64] Y. Yang, J. Ouyang, L. Ma, R. J. H. Tseng, C. W. Chu, *Adv. Funct. Mater.* **2006**, *16*, 1001.

[65] G. R. Whittell, I. Manners, *Adv. Mater.* **2007**, *19*, 3439.

[66] G. R. Whittell, M. D. Hager, U. S. Schubert, I. manners, *Nat. Mater.* **2010**, *10*, 176.

[67] C. Su, Y. Ye, L. Xu, C. Zhang, *J. Mater. Chem.* **2012**, *22*, 22658.

[68] S. -H. Hsiao, H. -M. Wang, P.-C. Chang, Y.-R. Kung, T.-M. Lee, *J. Polym. Res.* **2013**, *20*, 154.

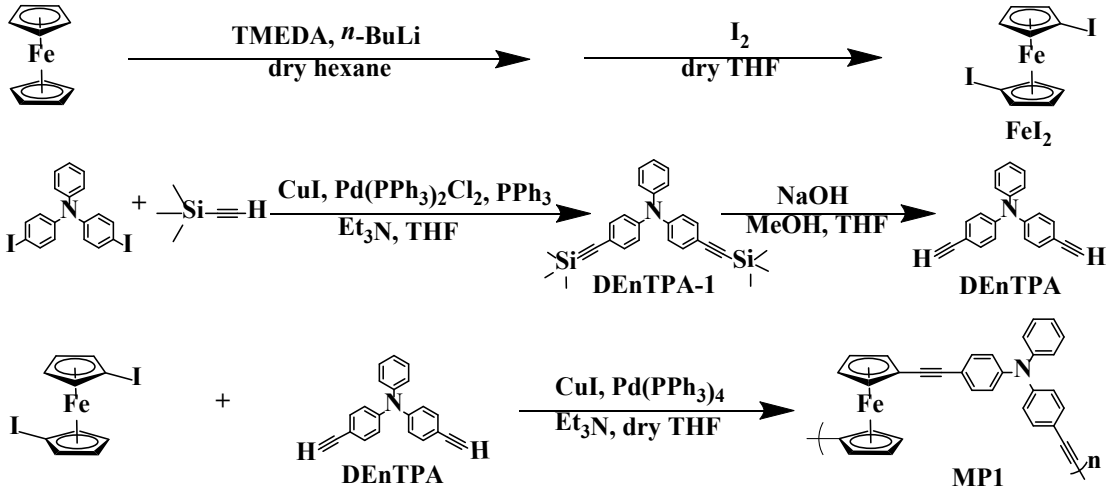

Scheme 1. Schematic representation of the synthesis of FeI_2, DEnTPA and MP1.

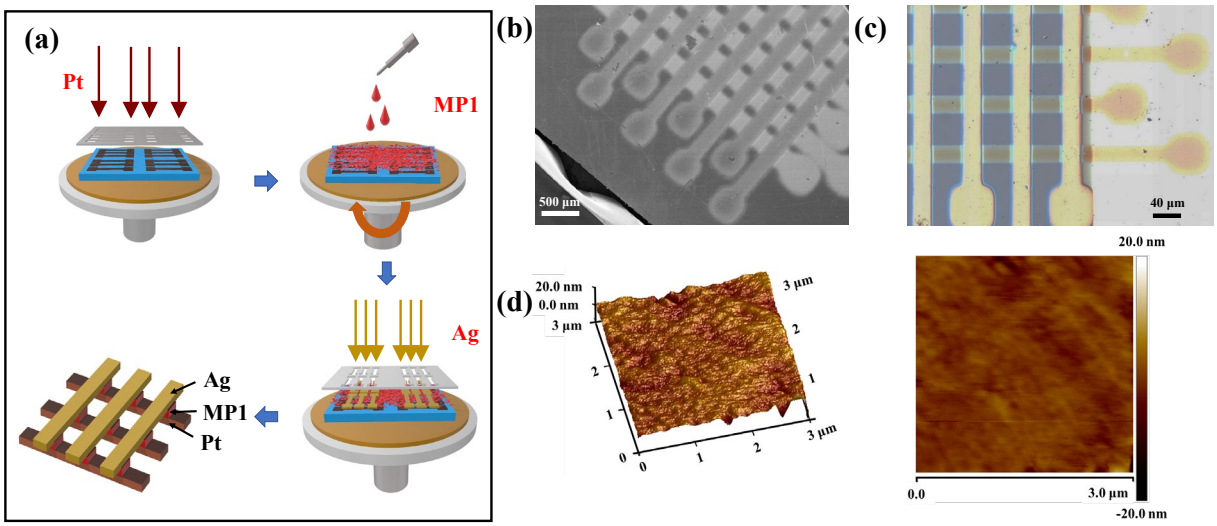

Figure 1. The physical characterization of Ag/MP1/Pt memristor. a) The whole process of the preparation of Ag/MP1/Pt memristor. b) The scanning electron microscope (SEM) picture of the crossbar structure of Ag/MP1/Pt memristor. c) The optical microscope (OM) of the crossbar structure of Ag/MP1/Pt memristor. d) The atomic force microscope (AFM) image of MP1 film.

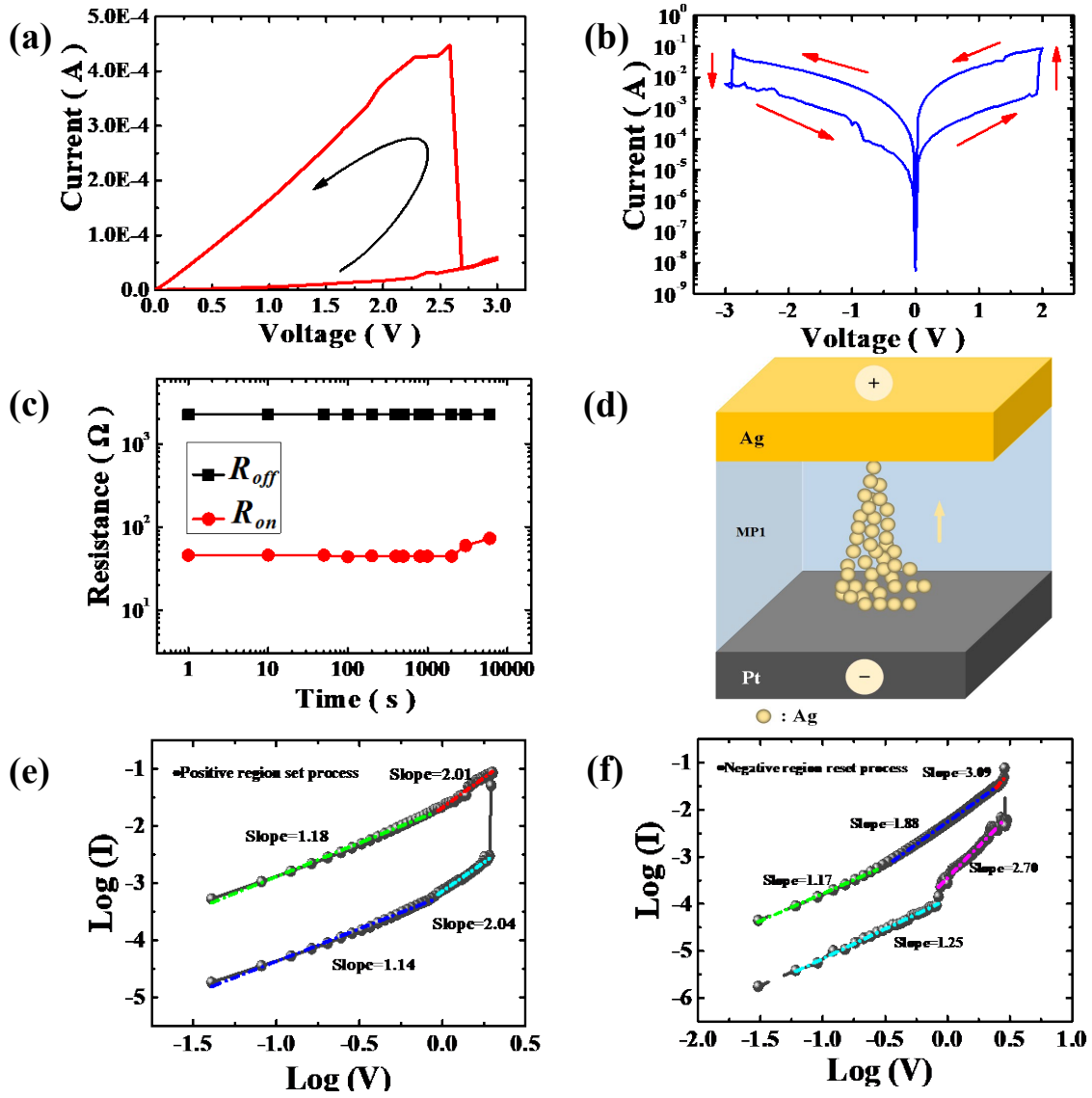

Figure 2. The electrical properties of MP1 memristor. a) The forming process of Ag/MP1/Pt. b) The typical *I-V* curve of Ag/MP1/Pt memristor. The value of Y-axis has been taken as logarithm. c) The retention of resistance of Ag/MP1/Pt memristor. d) The schematic diagram of the formation of conductive filaments in Ag/MP1/Pt device. Fits to log (*I*)-log (*V*) curves of the Ag/MP1/Pt using the SCLC model, showing e) the SET process and f) the RESET process. Fitted slopes are indicated.

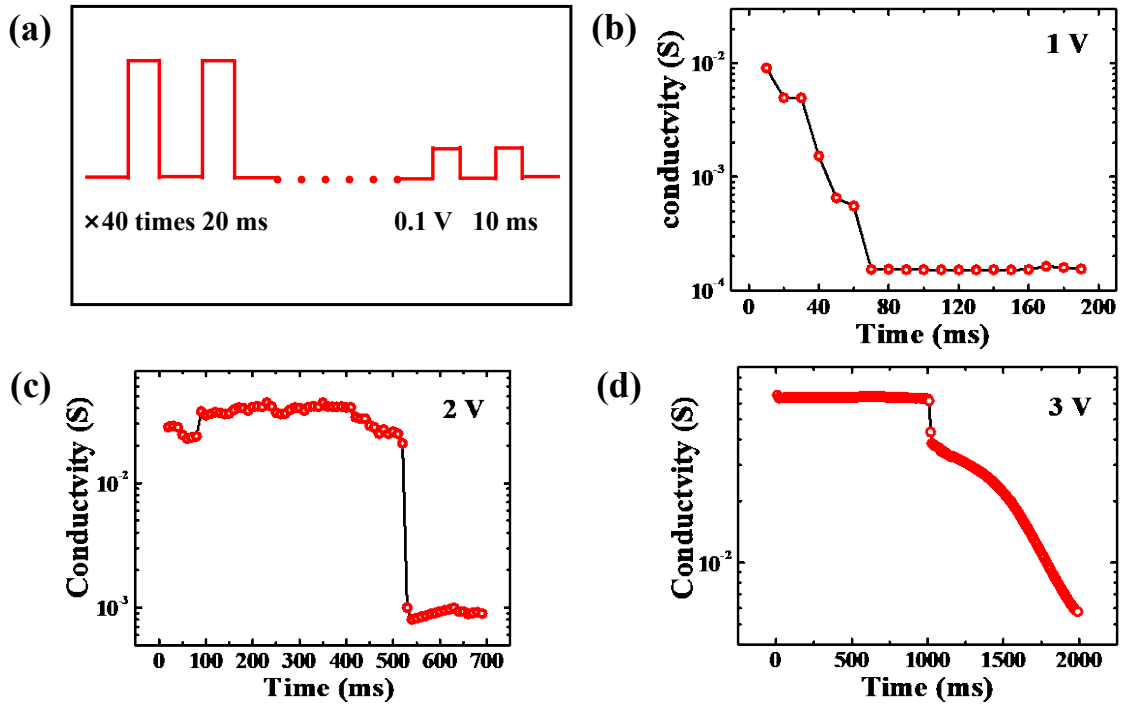

Figure 3. Pulse experiments of transferring from temporary short-term memory (STM) to a permanent long-term memory of Ag/MP1/Pt memristor. a) The schematic diagram of the continuous pulse of applied voltage and the read voltage. b) The process of the change of conductivity of MP1 memristor after the simulation of an applied voltage of 1 V. c) The process of the change of conductivity of MP1 memristor after the simulation of an applied voltage of 2 V. d) The process of the change of conductivity of MP1 memristor after the simulation of an applied voltage of 3 V.

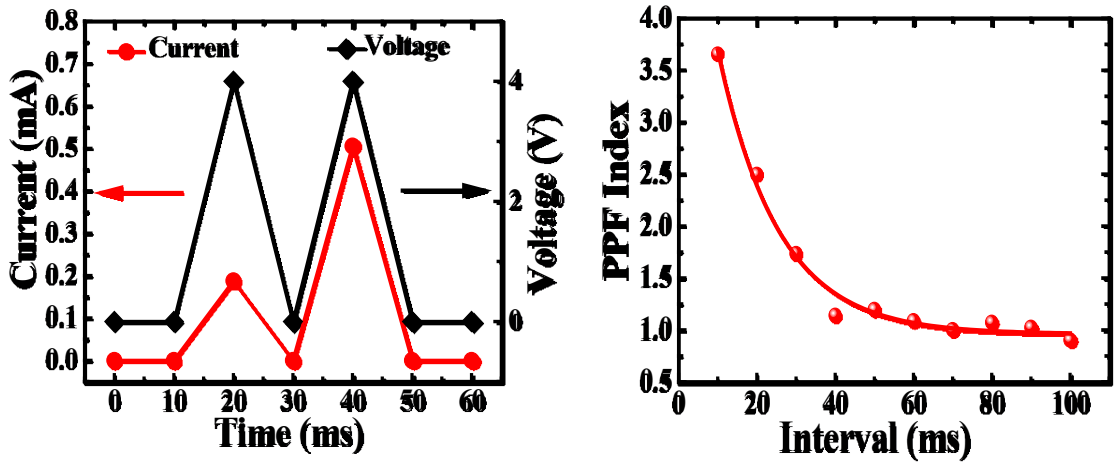

Figure 4. The relationship between the double pulse facilitation index and the pulse interval and the fitting map.

The table of contents

A new metallopolymer MP1 containing ferrocene and triphenylamine has been designed and synthesized, which was utilized as the active layer of memristor with electrodes of Ag and Pt. MP1 has been found to act as metal-ions-accommodation site and has great potential to help the formation of conductive filaments in active region. Additionally, synaptic functions have been successfully emulated using MP1 memristor.

Keywords: donor-acceptor, metallopolymer, memristor, brain-inspired systems, memory device

Donor-Acceptor Metallopolymers Containing Ferrocene for Brain Inspired Memristive Devices

Miaocheng Zhang, Chenxi Ma, Dawei Du, Jing Xiang, Suhao Yao, Ertao Hu, Shujuan Liu, Yi Tong, Wai-Yeung Wong,* and Qiang Zhao**

ToC Figure

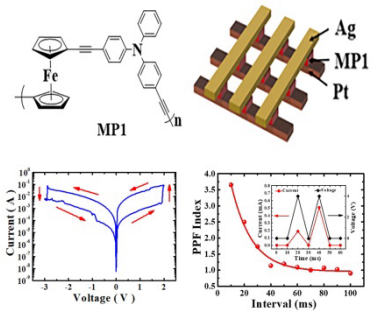

Supporting Information

Donor-Acceptor Metallopolymers Containing Ferrocene for Brain Inspired Memristive Devices

Miaocheng Zhang, Chenxi Ma, Dawei Du, Jing Xiang, Suhao Yao, Ertao Hu, Shujuan Liu, Yi Tong, Wai-Yeung Wong,* and Qiang Zhao**

C. Ma, S. Liu, Q. Zhao*
Key Laboratory for Organic Electronics and Information Displays & Jiangsu Key Laboratory for Biosensors, Institute of Advanced Materials (IAM), Nanjing University of Posts and Telecommunications (NJUPT)
9 Wenyuan Road, Nanjing 210023, Jiangsu, P.R. China
E-mail: iamqzhao@njupt.edu.cn
College of Electronic and Optical Engineering & College of Microelectronics, Institute of Flexible Electroncs (Future Technology), Nanjing University of Posts and Telecommunications (NJUPT)
9 Wenyuan Road, Nanjing 210023, Jiangsu, P.R. China
E-mail: tongyi@njupt.edu.cn
W.-Y. Wong*
Department of Applied Biology and Chemical Technology, The Hong Kong Polytechnic University (PolyU)
Hung Hom, Hong Kong, P. R. China
PolyU Shenzhen Research Institute
Shenzhen 518057, P. R. China
E-mail: wai-yeung.wong@polyu.edu.hk
J. Xiang, W.-Y. Wong*
Department of Chemistry, Hong Kong Baptist University
Waterloo Road, Hong Kong, P. R. China

Contents

Part I. Experimental Section

General Experimental Information: All materials for chemical synthesis were purchased from Sigma-Aldrich, J&K or Acros Organics and used without further purification. Commercially available reagents were used as received unless otherwise noted. The solvents used in the polymerization reactions were dried and distilled appropriately prior to use. ^{1}H NMR and ^{13}C NMR spectra were measured in deuterated solvents, and the instrument was a Bruker AV 400 MHz FT-NMR spectrometer, in which the chemical shift (δ in ppm) used tetramethylsilane as the internal standard of ^{1}H and ^{13}C nuclei. Fourier transform infrared (FT-IR) spectra were measured by a Perkin Elmer Paragon 1000 PC spectrometer, and KBr pellets were used for solid state spectroscopy. On the Agilent 1050 HPLC system with visible wavelength and fluorescent detector, the molar masses (M_n and M_w) and polydispersity indexes (PDIs) of polymers were examined by size exclusive chromatography (SEC). The UV-Vis absorption spectra were obtained on a HP-8453 diode array spectrophotometer. The photoluminescence (PL) spectra were measured with a PTI Fluorescence Master Series QM1 spectrophotometer. The electrochemical properties of MP1 were investigated by CV studies in the thin film state. Thicknesses of all thin layer electrodes were measured by the KLA-Tencor P6 surface analyzer. The electrochemical properties of MP1 were investigated by CV in thin film state. CV measurements of MP1 thin film on a glassy carbon electrode were taken in 0.1 M solution of tetrabutylammonium hexafluorophosphate (*n*-Bu_4NPF_6) in anhydrous DMF. The ferrocene/ferrocenium couple was used as the internal standard at a scan rate of 50 mV s^{-1} The electrical characteristics and pulse tests were carried out by the Keithley 4200A semiconductor analyzer. The scanning electron microscope (SEM) picture of the crossbar structure of Ag/MP1/Pt memristor was carried out by Hitachi S4800 with the ion-containing sputtering instrument E-1010. The optical microscope (OM) of the crossbar structure of Ag/MP1/Pt memristor was acquired by DM6000M of LECIA analyzer. The atomic force microscope (AFM) image of MP1 film was carried out by Dimension icon analyzer.

Synthesis

FcI_2 was synthesized according to a modified literature procedure.[1-3] An oven-dried 250 mL two-necked flask was charged with ferrocene (5.0 g, 26.9 mmol), tetramethyl ethylenediamine (10 mL, 67.2 mmol) and hexane (100 mL). When the resulting mixture was cooled to 0 ℃, 28 mL of the solution of n-BuLi (2.4 mol L^{-1}) in hexane was added dropwise under N_2 atmosphere. After being stirred for 12 h, the resulting bright orange suspension was cooled to -78 ℃ and a solution of I_2 (15.0 g, 59.2 mmol) in dry THF was added. The mixture was allowed to warm to room temperature (r. t.) and continued to stir for 2 h. Then the reaction mixture was quenched with the solution of $Na_2S_2O_3$ (100 mL) and stirred for 15 min. The organic phase was separated and dried over Na_2SO_4 after which the solvents were removed under vacuum. After the flash column chromatography, a dark red crude oil, containing FcI_2 accompanied by minor amounts of ferrocene and monoiodo-substituted ferrocene FcI was obtained (7.6 g). The crude product was extracted by n-hexane and $FeCl_3$ aqueous solution (0.5 mol L^{-1}). When Fc/FcI contaminants had been removed, the organic phase was washed with water, dried over Na_2SO_4, filtered and evaporated to a dark red oil. The product was further purified via silica gel chromatography by using hexane as eluent to afford a dark oil (2.5 g, 21%).^{1}H NMR ($CDCl_3$, 400 MHz): δ 4.37 (*pseudo*-t, 4H, J = 1.6 and 2.0 Hz, C_pH), 4.18 (*pseudo*-t, 4H, J = 2.0 Hz, C_pH). ^{13}C NMR ($CDCl_3$, 100 MHz): δ 77.59 (C_pI, CH), 72.28 (C_pI, CH), 40.29 (C_pI, CI).

DEnTPA-1 was synthesized according to a modified literature procedure.[4] A mixture containing 4,4'-diiodotriphenylamine (6.0 g, 12.1 mmol), CuI (115 mg, 0.6 mmol), $Pd(PPh_3)Cl_2$ (421 mg, 0.6 mmol), triethylamine (30 mL) and THF (30 mL) was degassed at r.t. for 30 min and then trimethylsilylacetylene (5.2 mL, 36.3 mmol) was injected under N_2. After being stirred for another 30 min, the reaction mixture was heated to 50 ℃ and stirred overnight. Water was added to quench the reaction and CH_2Cl_2 was used for extraction (50 mL×3). The organic layer was collected, dried over anhydrous Na_2SO_4, filtered and

concentrated under reduced pressure to give the crude product, which was purified over silica gel chromatography using hexane/CH_2Cl_2 (10:1, v/v) as eluent to afford a light-yellow sticky solid (4.3 g, 81%). ^{1}H NMR (CD_2Cl_2, 400 MHz): δ 7.35~7.28 (m, 6H), 7.13~7.07 (m, 3H), 6.99~6.95 (m, 4H). 0.23 (s, 18H). ^{13}C NMR (CD_2Cl_2, 100 MHz): δ 147.97, 147.10, 133.40, 130.10, 126.16, 124.86, 123.64, 117.47, 105.52 (ArC), 93.95 (C≡C), 0.24 (Si (CH_3)$_3$).

DEnTPA was synthesized according to a modified literature procedure.[4] A solution of DEnTPA-1 in THF (50 mL) and methanol (50 mL) was treated with NaOH (936 mg, 23.4 mmol). The mixture was stirred at r. t. overnight. After the solvent was removed under reduced pressure, the crude product was purified by a flash chromatography with hexane/CH_2Cl_2 (10:1, v/v) as eluent to afford the pure product as a light-yellow viscous oil (87%). ^{1}H NMR ($CDCl_3$, 400 MHz): δ 7.37~7.34 (m, 4H, ArH), 7.31~7.27 (m, 2H, ArH), 7.12~7.08 (m, 3H, ArH), 7.01~6.98 (m, 4H, ArH), 3.04 (s, 2H, C≡CH). ^{13}C NMR ($CDCl_3$, 100 MHz): δ 147.85, 146.77, 133.42, 129.82, 125.80, 124.56, 123.39, 116.16, 116.16 (ArC), 83.85 (ArC≡C), 76.82 (C≡CH).

References:

[1] M. Roemera, C. A. Nijhuis, *Dalton Trans.* **2014**, *42*, 11815.

[2] D. A. Khobragade, S. G. Mahamulkar, L. Pospíšil, I. Císarová, L. Rulíšek, U. Jahn, *Chem. Eur. J.* **2012**, *18*, 12267.

[3] M. S. Inkpen, S. Du, M. Driver, T. Albrecht, N. J. Long, *Dalton Trans.* **2013**, *42*, 2813.

[4] Z. Fang, M. Samoc, R. D. Webster, A. Samoc, Y.-H. Lai, *Tetrahedron Lett.* **2012**, *53*, 4885.

Part II. Supplementary Tables and Figures

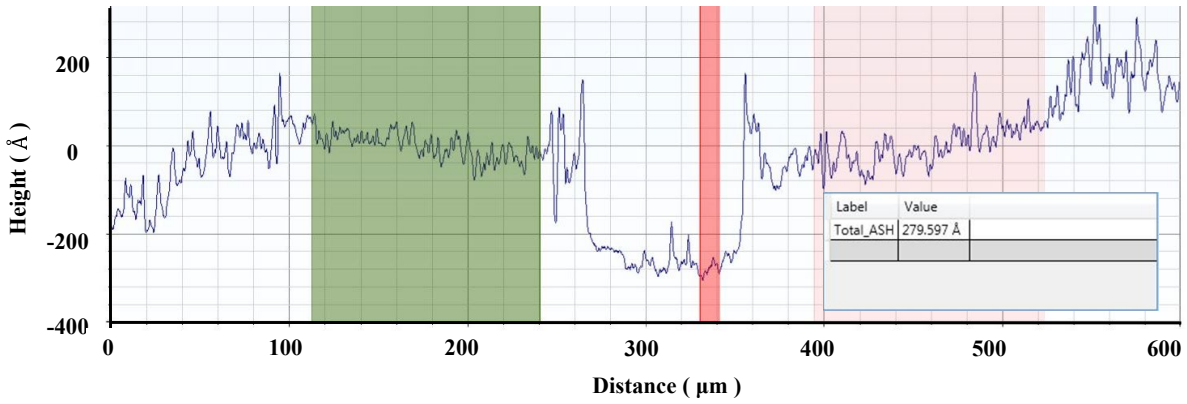

Figure S1. The measurement of the thickness of MP1 film by probe type profilometer.

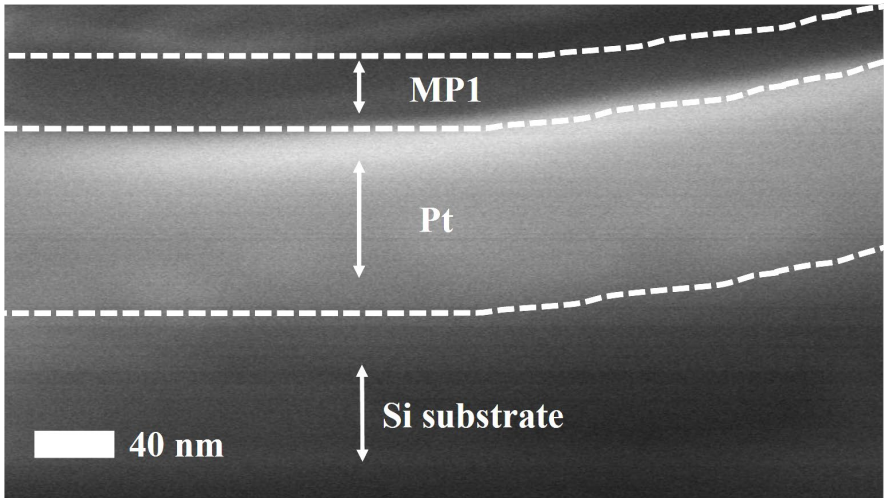

Figure S2. The SEM picture of the sectional structure of MP1 film on the substrate.

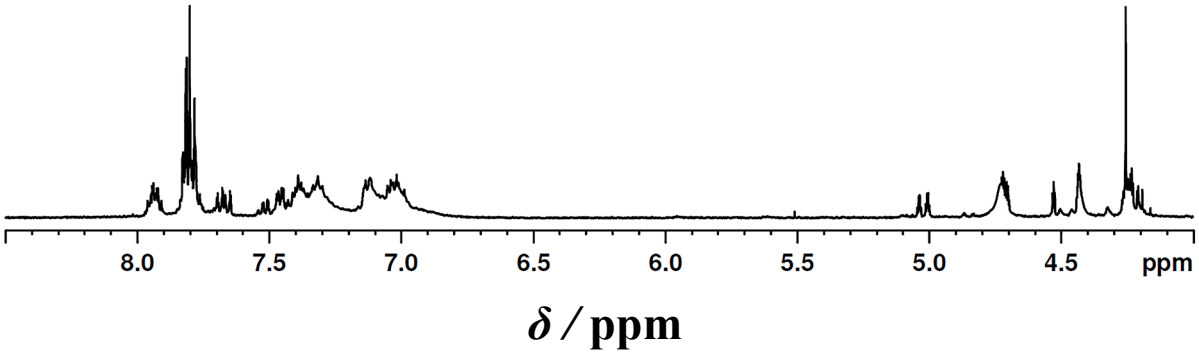

Figure S3. ^{1}H NMR spectrum of FcMMP1 in THF-*d8*.

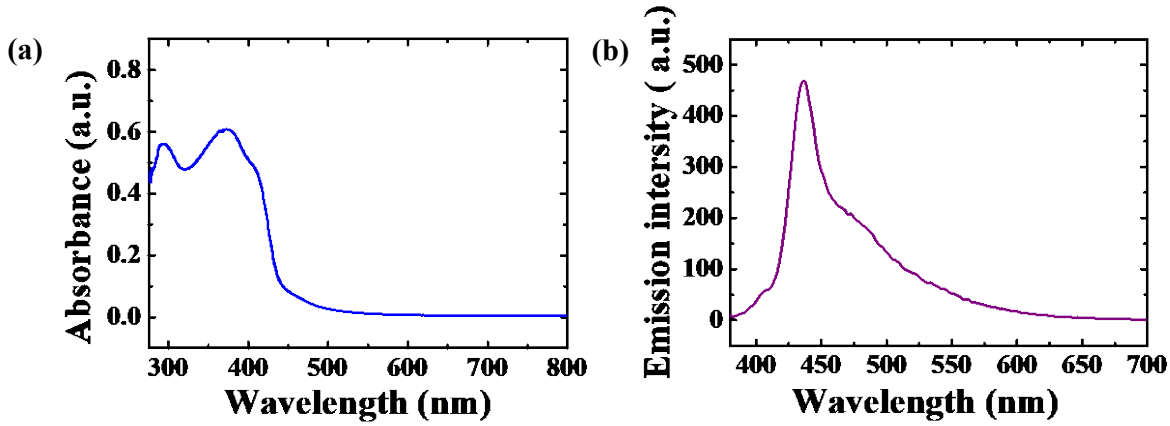

Figure S4. a) UV absorption spectra of MP1 in THF. b) PL spectra of MP1 in THF.

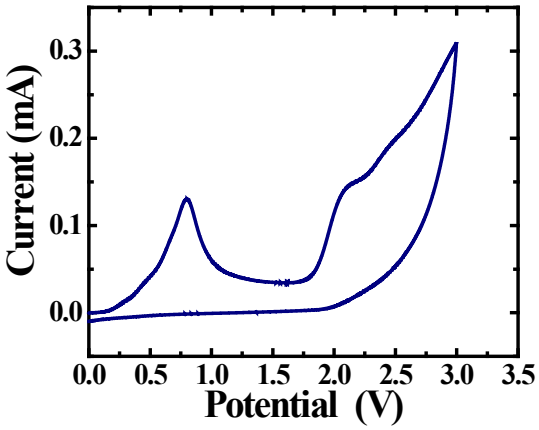

Figure S5. CV curves of MP1 in 0.1 mol L^{-1} TBAP DMF solution.

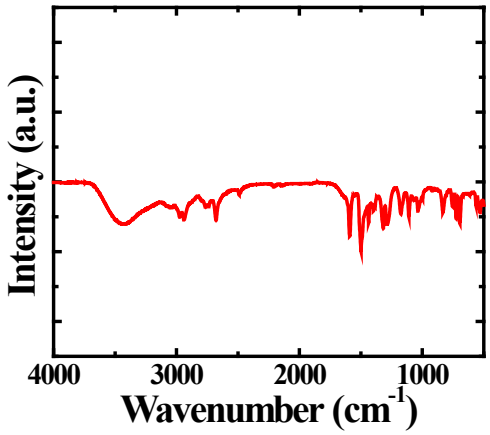

Figure S6. FT-IR spectra of MP1 by using KBr pellet method.

Table S1. Molecular masses and PDI of MP1 via SEC in the THF solution.

Polymer	M_n(g mol^{-1})	M_w(g mol^{-1})	PDI(M_w/ M_n)
MP1	5.6×10^3	9.7×10^3	1.7

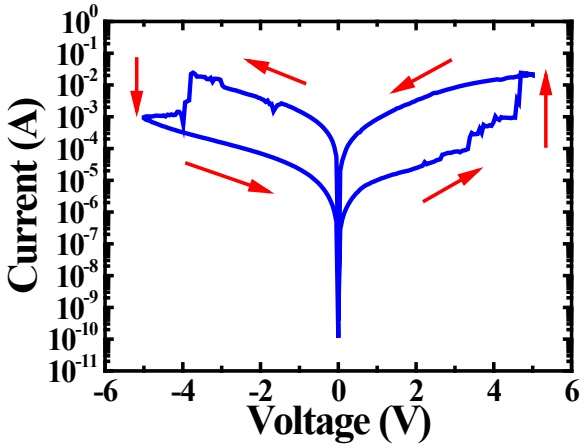

Figure S7. The typical *I-V* curve of Ag/MP1/SiO_2/Pt memristor.

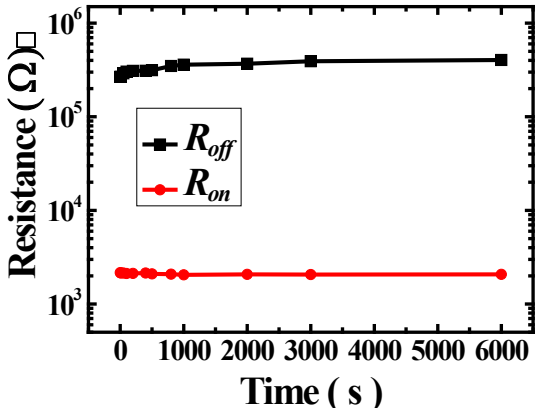

Figure S8. The retention of the resistance of Ag/MP1/SiO_2/Pt memristor.

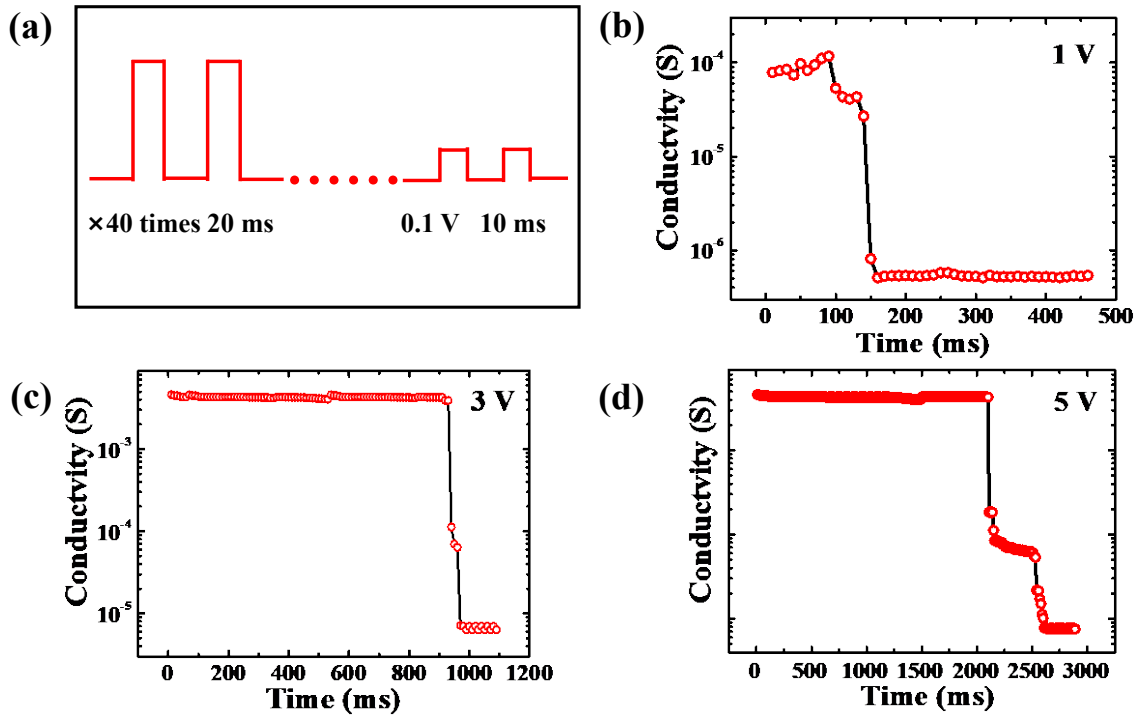

Figure S9. Pulse experiments of transferring from temporary short-term memory (STM) to a permanent long-term memory of Ag/MP1/SiO_2/Pt memristor. a) The schematic diagram of the continuous pulse of applied voltage and the read voltage. b) The process of the change of conductivity of MP1 memristor after the simulation of an applied voltage of 1 V. c) The process of the change of conductivity of MP1 memristor after the simulation of an applied voltage of 3 V. d) The process of the change of conductivity of MP1 memristor after the simulation of an applied voltage of 5 V.

Table S2. Fitting parameters of the functional relationship between PPF index and pulses intervals.

Parameter	A_1	T_1	Y_0
The fitting value	5.22	30.88	0.96

Part III. Supplementary Statements

In order to save the power consumption, we tried to introduce the SiO_2 layer into Ag/MP1/Pt memristor. The typical *I-V* characteristic of Ag/MP1/SiO_2/Pt is shown in **Figure S**7. The memristors were initially at the HRS. When the applied voltage was swept to 5 V, there was a jump in the current of the device. When the applied voltage was swept from 5 V to 0 V, LRS was maintained due to the formation of conductive channels. Correspondingly, when the negative voltage was applied to the device, the device would return to the HRS. It can be found that the working current of Ag/MP1/SiO_2/Pt device is one order less than the device without SiO_2. It is obvious that the working current of the devices has indeed been lower than the devices without SiO_2. But the time of the switching from HRS to LRS and the set voltage have increased obviously. So, the issue of power consumption has not been completely solved by introducing the SiO_2 layer to Ag/MP1/Pt memristors.